Research Article Vol. 32, No. 24 / 18 Nov 2024 / Optics Express 42383
Optics EXPRESS

Device optimization of all-perovskite triple-junction solar cells for realistic irradiation conditions

MOHAMED HUSSEIN,[1,2,*] FABRIZIO GOTA,[1,3] ULRICH W. PAETZOLD,[1,3] AND ULI LEMMER[1,3]

[1]*Light Technology Institute, Karlsruhe Institute of Technology, 76131 Karlsruhe, Germany*
[2]*Department of Physics, Faculty of Science, Ain Shams University, Abbassia 11566, Cairo, Egypt*
[3]*Institute of Microstructure Technology, Karlsruhe Institute of Technology, Hermann-von-Helmholtz-Platz1, 76344 Eggenstein-Leopoldshafen, Germany*
[*]*Mohamed.Hussein@kit.edu*

Abstract: All-perovskite two-terminal tandem solar cells, comprising two or more junctions, offer high power conversion efficiencies (PCEs) that exceed the limits of single-junction photovoltaics. Realizing high-efficiency SCs requires carefully optimizing the photoactive layer, front electrodes, and functional layers. Here, we first aim to determine the optimal device architecture, i.e., the perovskites bandgaps and optimum layer thicknesses, for standard test conditions (STCs). We then optimize the energy yield (EY) under realistic outdoor conditions (ROCs), i.e., the overall electrical energy to be expected in one year at a specific location. In the first step, we reference our simulation with two terminal all-perovskite triple-junction SCs (2T3J-PSCs) to previously experimentally realized PSC with a PCE of 20.1% as a benchmark to derive the underlying diode parameters and use our in-house energy yield code combined with a hybrid particle swarm optimization and gravitational search algorithm (PSOGSA) to find the optimal bandgap combination and perovskite layer thicknesses. The optimized SCs with the optimal bandgap combination offer a PCE of 25.1% with a current density of 10.1 mA/cm^2. Furthermore, the effect of the other functional layers, such as transparent conductive oxide (TCO), hole transport layer (HTL), and recombination junctions (RJs), is also investigated to enhance the cell performance further. The SCs with optimized layers exhibit improved parameters: PCE of 27.1%, with a relative improvement of 34.8% in the PCE compared with the fabricated cell, and a high current matching a of 10.8 mA/cm^2. The numerical results showed that the reported cell can potentially achieve a PCE of 36% at an eV_{oc}/E_G ratio of 0.72. However, the optimal parameters may vary in real-world operating conditions due to variations in temperature, humidity, and light exposure. As a result, the optimal energy yield (EY) parameters may differ. Therefore, the energy yield optimizing process is also carried out by considering ROCs in Phoenix, AZ, USA, to find the best parameters under these conditions. We found that the optimum top layer bandgap under ROCs is lower than under STCs due to a bluer, more shifted spectrum in ROCs. After that, the optimized cell under ROCs is tested in several locations exhibiting different climatic conditions (Seattle, Honolulu, Los Angeles, Miami, and Milwaukee). The numerical results show that the optimized cell under ROCs offers an increase in energy yield in several locations compared to conventional single-junction crystalline Si-SCs (PCE = 23.6%) with a high energy yield of 648.2 kWh/m^2 in Phoenix, with an improvement of 39.9% in the EY compared to the Si-SC counterpart. Our results provide design guidelines for fabricating a highly efficient triple-junction perovskite SC in the lab and outdoor applications and improve the efficiency of 2T3J-PSCs beyond the 30% limit.

#537577 https://doi.org/10.1364/OE.537577
Journal © 2024 Received 30 Jul 2024; revised 14 Oct 2024; accepted 18 Oct 2024; published 5 Nov 2024

Optics EXPRESS

1. Introduction

The previous decades have seen consistent enhancements in the performance and affordability of photovoltaic (PV) technologies [1], making it a competitive method of generating electricity with minimal GHG emissions. Nevertheless, reducing the levelized cost of electricity (LCOE) from PV is still crucial. Improving the power conversion efficiency (PCE) is a high priority for achieving this objective [1,2]. In this context, silicon-based solar cells (SCs) have achieved commercial success and a record PCE of 26.7% [3]. These record values approach the maximum theoretical efficiency of a single-junction SC under ideal conditions, i.e., the Shockley-Queisser limit of 33% [4]. To surpass this limit, tandem/multijunction SCs provide a low-cost and effective solution [5]. In this regard, impressive PCEs of 32.8%, 37.9%, and 39.2% have been achieved for double-junctions, triple-junctions, and six-junction tandem SCs, respectively, utilizing III−V compound semiconductors. However, their expensive and intricate manufacturing process limits their application to space satellites or concentrator PV [6,7]. Therefore, developing high-efficiency and cost-effective multijunction SCs is crucial. Multijunction perovskite solar cells (PSCs) might offer a solution as they can potentially be fabricated at low costs [8].

Since the initial success of organic-inorganic metal halide perovskite-based SCs in 2009 [9], they have shown excellent properties such as defect tolerance, high charge carrier mobility, low trap density, and small exciton dissociation energy [8]. Additionally, their bandgaps can be tuned from ≈1.17 to 2.3 eV by adjusting the composition of the A cation, B metal, and X halide anion within ABX_3 crystal structure, making them ideal candidates for use in all-perovskite tandem SCs [10]. Recent developments in PSC technology have led to the creation of all-perovskite double junction (2J) or triple junction (3J) SCs, which have the potential to achieve higher PCE than single-junction PSCs. These 2J or 3J multijunction SCs are also highly attractive due to their low-temperature solution processing and ease of scalability, making them suitable for lightweight, low-cost, and flexible applications [11]. Recent experimental studies have demonstrated promising efficiencies in all-perovskite-triple-junction solar cells (3J-PSC). In this context, Wang *et al*. [12] achieved a PCE of 16.8% for monolithic 3J-PSC with a combination of 1.73 eV, 1.57 eV, and 1.23 eV perovskite sub-cells. Further, Xiao *et al*. [13] reported a solution-processed 3J-PSC with PCE of 20.1% through the engineering of perovskite bandgaps and interconnecting layers. The perovskite layers exhibited bandgaps of 1.99 eV, 1.60 eV, and 1.22 eV for the front, middle, and back subcells, respectively. Furthermore, Wang *et al*. [14] fabricated 3J-PSC with 2 eV, 1.60 eV, and 1.22 eV bandgaps. The reported cell achieved a PCE of 24.3% (23.3% certified quasi-steady-state efficiency) with an open-circuit voltage of 3.21 V. Shrivastav *et al*. [15] recently simulated 3J-PSCs with bandgaps of 1.99 eV, 1.60 eV, and 1.20 eV. The optimized cell offers a PCE of 26.2%. However, the reported efficiencies are still far from a triple junction device's theoretical efficiency limit of 49% [16]. Optimizing the thicknesses and bandgaps of the top, middle, and bottom cells is essential to utilize the full potential of 3J-PSC. Therefore, this study is dedicated to finding the optimum bandgaps and thicknesses for such devices under standard tests and real-world conditions.

Today, optimization techniques are essential tools for engineers in many fields [17]. Therefore, many meta-heuristic optimization techniques, such as genetic algorithm (GA) [18], particle swarm optimization (PSO) [19], and gravitational search algorithm (GSA) [20], have been performed successfully in different engineering design tasks. Hybrid algorithms have been proposed to balance the overall exploration and exploitation capabilities to improve the convergence capability of optimization techniques [21]. PSO is one of the most widely used evolutionary algorithms in hybrid methods due to its simplicity, convergence speed, and ability to search for a global optimum. Some studies in the literature have been done to combine the PSO with other algorithms, such as GA, differential evolution, and ant colony optimization. These hybrid algorithms aim to improve the convergence capability and reduce the probability of trapping in a local optimum. A new hybrid population-based algorithm combining PSO and GSA has recently been proposed.

Optics EXPRESS

The main idea is to integrate the ability of exploitation in PSO with the ability of exploration in GSA to synthesize both algorithms' strengths. A set of various standard benchmark functions was examined. Hybrid GSA-PSO algorithm typically escape from local optimums with faster convergence than the standard PSO and GSA [21].

In this work, extensive optical and electrical simulations are conducted utilizing an internally developed energy yield (EY) simulation tool called EYcalc, made publicly available as open-source software [22,23]. The in-house EY code is linked with the hybrid particle swarm optimization and gravitational search algorithm (PSOGSA) to find the optimum perovskite layer thicknesses and band gaps [24]. The optimization process is carried out to increase SC-PCE and achieve the current matching between the subcells under STC. First, we start to simulate the optical and electrical characteristics of the reported cell by modelling the high-efficiency 3J-PSC presented by Xiao *et al.* [13] as a benchmark. Further, a comprehensive study is conducted to reduce the loss mechanisms within the optimum cell architecture. Second, we study the effect of changing the transparent conductive oxide (TCO), hole transport layer (HTL), and recombination junctions (RJs) to achieve the highest possible efficiency for a 3J-PSC. Third, electrical optimization is carried out to increase the PCE of the optimized cell. The electrically optimized cell offers a PCE of 36% under STCs with an enhancement of 79% compared to the previously reported value by Xiao *et al.* [13]. Current matching is of utmost importance in achieving this. Achieving such matching is possible under a standardized solar spectrum with direct illumination. However, in real-world conditions, the spectrum of sunlight and the diffuse-to-direct sunlight ratio varies significantly depending on the location and weather conditions. Therefore, we conducted a study to determine the optimum bandgaps under ROCs and understand the impact of changes in the spectral composition of sunlight on 3J-PSC. Our findings show that the top perovskite subcell bandgap shifted under ROCs is lower than under STC. Additionally, we compared the EY of the suggested 3J-PSC with that of the Si-SC in different locations across various climatic zones in the United States. Our research shows that 3J-PSC with optimum bandgaps offers a high EY of 648.2 KWh/m^2 in Phoenix, AZ, USA, with a relative improvement of 39.9% compared to the Si-SC counterpart. Furthermore, our work indicates that the energy yield is always higher for the 3J-PSC than the c-Si SC, regardless of specific climatic and insolation conditions.

2. Simulation methodology

This study aims to find the optimal device architecture, specifically the perovskites' bandgaps and optimum layer thicknesses, for standard test conditions (STCs) and realistic outdoor conditions (ROCs). To achieve this, we first study and simulate an all-perovskite triple-junction architecture with bandgaps of 1.99 eV, 1.6 eV, and 1.22 eV for the top, middle, and bottom perovskite absorber layers. This architecture is similar to the previously fabricated and measured cell by Xiao *et al.* [13]. Figure 1(a) shows the device architecture used in our simulation study. Every perovskite subcell is sandwiched between an HTL and the electron transport layer (ETL) to form the p-i-n architecture. The top one (1.99 eV bandgap) is situated between the PTAA and C_{60} as HTL and ETL layers, respectively. The middle subcell is sandwiched between a NiO/PTAA bilayer HTL and C_{60} as the ETL. The bottom subcell with a lower bandgap of 1.22 eV is sandwiched between PEDOT:PSS and BCP as HTL and ETL, respectively. A SnO_2 thin film protects the cell from damage during the deposition of the solution-processed 1.22 eV subcell. A 1 nm gold is employed as a recombination junction (RJ) to facilitate electron-hole recombination between the top and bottom subcells. The numerical study is carried out using an in-house developed energy yield (EY) modeling platform [17]. To find the optimal band gaps and the thicknesses of the perovskite absorber layers, the EY code is integrated with the hybrid particle swarm optimization and gravitational search algorithm (PSOGSA) [18,23]. Figure 1(b) illustrates the simulation and optimization strategy. The bandgap of the bottom subcell is kept constant at 1.22 eV, which is

Optics EXPRESS

currently the lowest achievable perovskite bandgap in efficient SC. In contrast, the bandgap of the middle subcell varies from 1.48 eV to 1.68 eV, and the top sub-cell bandgap varies from 1.90 eV to 2.3 eV. For every simulation study, the optimizer changes the three perovskite layer thicknesses (d_1, d_2, and d_3) between the lower and upper limits of 180 nm to 1000 nm, respectively, while the other layers' thicknesses are fixed at the initial thicknesses are provided in Table 1. Increasing the thickness further will render it comparable to the charge carrier diffusion length, leading to inefficient charge carrier extraction and, consequently, a drop in the fill factor and V_{oc}. The optimizer randomly generated the values of d_1, d_2, and d_3 and employed them as input to the EY code. Then, the code calculates the absorption, short circuit current density, and PCE. This loop iterates until the results converge. The PCE is calculated under standard test conditions (AM1.5) and employed as a fitness function for the GSA-PSO technique. The PCE is calculated by

$$\text{Fitness function (PCE)} = \frac{P_m}{P_{in,STC}} = \frac{P_m}{1000\ W/m^2} \tag{1}$$

where P_m is the solar cell's output power at maximum power point under AM1.5.

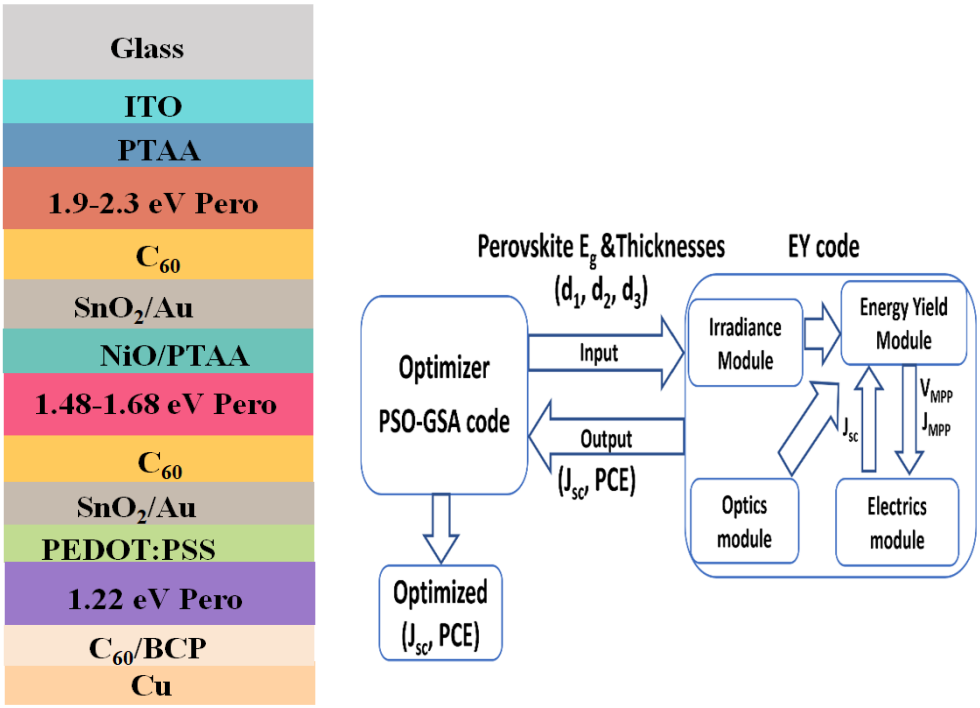

(a) (b)

Fig. 1. (a) Modified 3J-PSC device architecture reported in [13], (b) The simulation and optimization strategy.

Optics EXPRESS

Table 1. Tabulated materials thicknesses for all-perovskite triple junction (3J-PSC) architecture reported in [13]

Materials	Thickness range (nm)
ITO	100 nm
PTAA	8
Top: Perov. E_G(1.99 eV)	250
C_{60}	20
SnO_2	25
Au(recombination)	1
NiO/PTAA	80/8
Middle: Perov. E_G(1.60 eV)	560
C_{60}	20
SnO_2	25
Au(recombination)	1
PEDOT: PSS	30
Bottom: Perov. E_G (1.22 eV)	900
C_{60}	20
BCP	7
Cu	200

3. Hybrid GSA-PSO technique

The GSA-PSO technique, combines the advantages of the social thinking ability (g_{best}) of PSO with the local search capability of GSA and is applied in this study to optimize the thicknesses of perovskite layers and increase the PCE. In the PSO-GSA algorithm, the agents (perovskite layer thicknesses) are considered objects, and their performances are measured by their masses (PCEs). Objects with heavy masses represent good solutions. Each object attracts every other

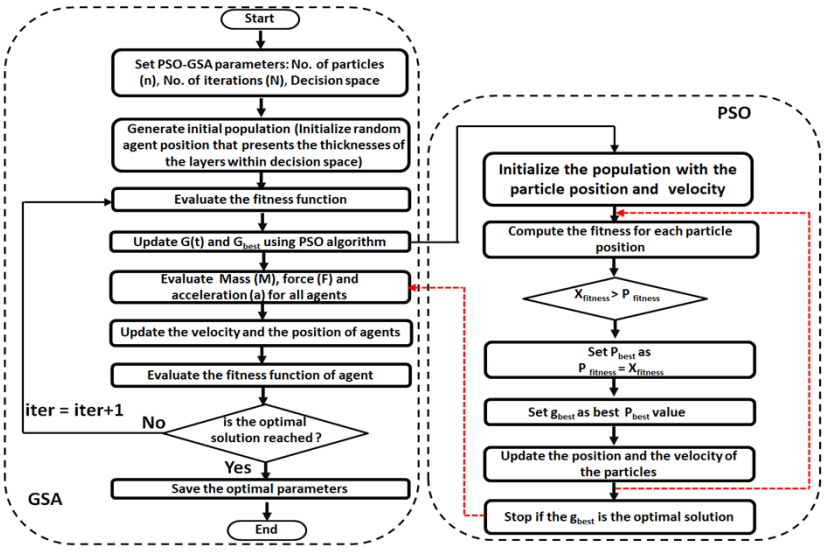

Fig. 2. Flow chart of hybrid PSO-GSA algorithm.

Optics EXPRESS

object with a gravitational force. Figure 2 shows the hybrid PSO-GSA flow chart [25]. The details of how the PSO-GSA algorithm operates are thoroughly explained in Supplement 1 S1. In this investigation, the algorithm is employed with 20 agent sizes and 50 iterations with a total evaluation number of only 1000. The decision space of the thicknesses of three perovskite layers varies between 180 nm and 1000 nm.

4. Results and discussion

4.1. Model validation

To check the validity of our optical and electrical simulation models, we first simulated a device architecture that was experimentally realized and reported on by Xiao *et al*. [13] (see Fig. 1(a)). In their study, they fabricated 3J-PSC with a PCE of 20.1%. Figure 3 shows the experimental J–V curves [13] compared to the results from our electrical model. A good agreement is achieved between our simulations and the measured results in [13], confirming the accuracy of our model. The simulated all-perovskite solar cell showed a power conversion efficiency (PCE) of 20.09%, which is very close to the experimentally reached efficiency (20.1%). Consequently, we utilize our model to predict the electrical performance of the modified cells in the upcoming subsections. The electrical parameters are extracted from a fitting experimentally measured JV in [13]. These parameters include the ideality factor (n_{id}), shunt resistance R_{sh}, series resistance R_s, and dark saturation current density (J_0). In this study, J_0 for the top, middle, and bottom perovskite subcells are $1.07e^{-20}$ mA/cm^2, $2.46e^{-15}$ mA/cm^2, and $7.21e^{-11}$ mA/cm^2, respectively. Additionally, the values of R_s and R_{sh} are 2.5 Ω and 2500 Ω cm^2, respectively, while the $n_{id} = 1.1$ for the three perovskite subcells.

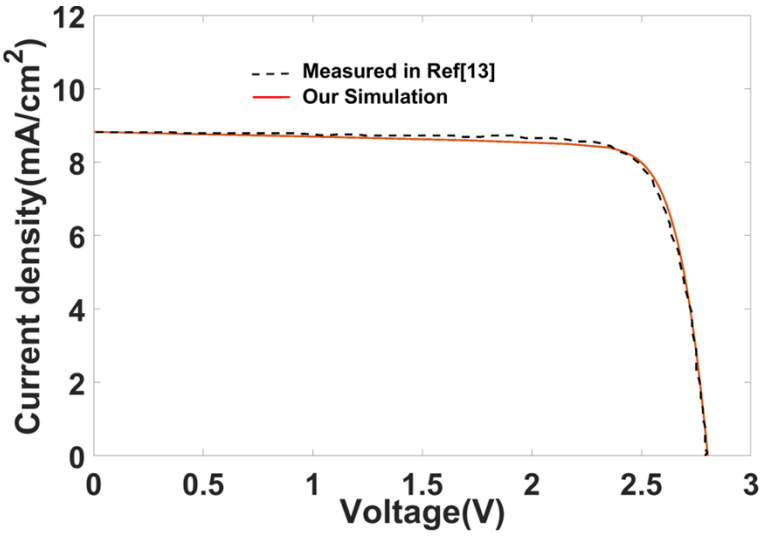

Fig. 3. J–V curves validation of our simulation and the real experimental J-V curve published in [13].

4.2. Optimal bandgaps under standard test conditions (STCs)

This study aims to find the optimal bandgaps of the top and middle perovskite layers in the stack shown in Fig. 1(a) under STCs. In this section, we explore the effect of changing the top perovskite layer bandgap from 1.90 eV to 2.3 eV while the middle layer varies from 1.48 eV to 1.68 eV. Meanwhile, the bottom perovskite subcell bandgap remains constant at 1.22 eV. In this

Optics EXPRESS

study, the three perovskite absorber layer thicknesses are varied by the optimizer between upper and lower limits of 180 nm and 1000 nm, which is experimentally feasible based. The other layer thicknesses (e.g., the transport layers) were fixed at the initial values, as listed in Table 1. Figure 4 illustrates the variation of the PCE under STCs with the bandgap's combination of the middle and top perovskite layers on the top of the fixed perovskite bottom layer with a 1.22 eV bandgap. It is noted that PCE larger than 23.5% requires the bandgap of the middle layer to exceed values of 1.6 eV, and the top layer's bandgap should exceed 2 eV. The minimum PCE of 20% is obtained at top cell and middle cell bandgaps of 1.48 eV and 2.3 eV. The maximum PCE of 25.1% is obtained when the top and middle perovskite bandgaps are 2.26 eV and 1.64 eV, respectively. The optimal thicknesses for the three perovskite layers are 828 nm, 822 nm, and 1000 nm for the top, middle, and bottom subcells, respectively. It is important to highlight that achieving these results using a full parametric sweep for the three layers from 180 nm to 1000 nm requires extensive computational processing and time, depending on the sweep steps, as indicated in Table 2 below. E.g., for a sweep step of 1 nm, more than $5{\cdot}10^8$ simulation runs are needed. However, utilizing the PSO-GSA optimization technique with 200 simulation runs has proven to be efficient, as shown in Figure (4) b. This is because optimization techniques like PSO-GSA offer a more targeted approach. By intelligently searching for the best solution based on a defined objective, they can often achieve similar results with significantly fewer iterations, effectively reducing the number needed to just 200 simulation runs. This significant reduction in computations enables the identification of the optimal configuration faster and more accurately. The suggested optimum cell offers a high PCE of 25%, higher than that of the fabricated cell in [13], with a PCE of 20.1% and a current of 8.8 mA/cm^2 suffering from current mismatching. It is worth stressing that our thickness and bandgap optimization have significantly improved the fabricated cell's PCE in [13] and [14] from 20% to 25.1%. At the same time, it provides a

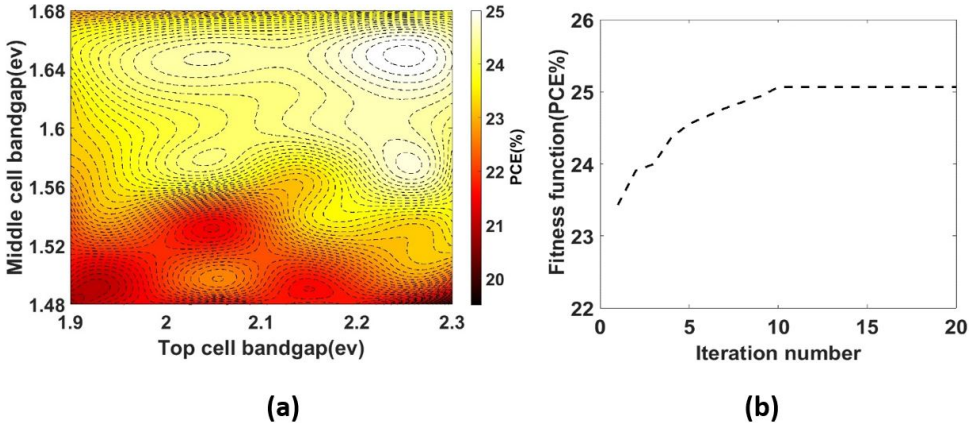

Fig. 4. (a) All 3J-PSC PCE as a function of the bandgaps of the middle and top perovskite layers on the top of the base perovskite absorber with a fixed bandgap of 1.22 eV under STC and (b) Fitness function versus the number of iterations for optimizing 3J-PSC PCE.

Table 2. Parametric sweeps at different sweep steps and number of simulations runs needed

Parametric sweep step for three perovskite layers thicknesses from 180 nm to 1000 nm	Total number of iterations needed
Sweep step 10 nm	83x 83 × 83 = 571,787 simulation runs
Sweep step 5 nm	165 × 165 × 165 = 4,492,125 simulation runs
Sweep step 1 nm	801 × 801 × 801 = 513,922,401 simulation runs

Optics EXPRESS

current matching between the 3J with a high value of 10.1 mA/cm^2. This enhancement is due to reduced reflection loss and the current matching between the three perovskite layers. Therefore, this study presents a comprehensive investigation that will be used as a guideline for fabricating any 3J-PSC; for any bandgap combinations for the top and middle perovskite layers. We provide the optimum thickness that will result in the highest efficiency and current matching. Table S1 in the Supplement 1 shows the thicknesses for each combination of bandgaps. Therefore, the optimized stack will be used in subsequent studies.

Figure 5(a) shows a comparison of the external quantum efficiency (EQE) for the previously fabricated cell in [13] and our reported optimized 3J-PSC with optimal bandgaps. The figure reveals that the 3J-PSC introduced here exhibits a higher EQE and an improved matched current density of 10.1 mA/cm^2 for the three subcells. Figure 5(b) illustrates the PCE for the cell in [13] and our optimized 3J-PSC, as well as for a 3J-PSC with ideal values of the series resistance and shunt resistance of 0Ω and 100 M Ω, respectively. A key observation from this figure is the significant impact of the R_s and R_{sh} values on the PCE, leading to a further increase up to 27.1%. This enhancement is directly linked to the increase in the fill factor. To further increase the PCE of the optimized cell (optimized with regard to the bandgaps), we need to gain insights into where the losses are occurring within the reported stack and identify possible improvements. We present the absorptance and the current density in all layers (c.f. Fig. 1). It can be seen from Fig. 6 that 11.1 mA/cm^2, 2.4 mA/cm^2, and 0.39 mA/cm^2 are lost in reflection losses, ITO parasitic absorption losses, and Au parasitic absorption losses, respectively. To address these losses, various functional layers are also optimized, and the results are shown in the Supplement 1, such as front electrode material and thickness (see Table S2, Figure S1), antireflection coating layer (see Table S3, Figure S4), recombination junctions (see Table S4, Figure S3), and hole transport layer (HTL) optimization (see Figure S4). This optimization further increased the PCE of the investigated cell to 27.1%.

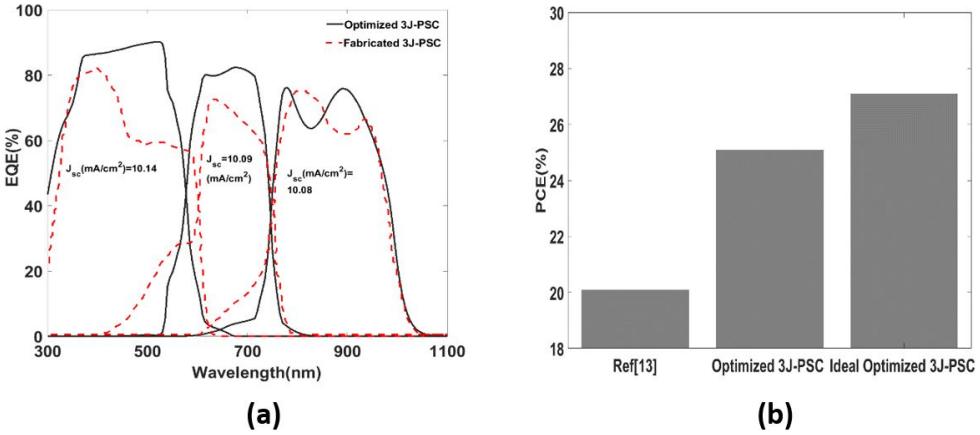

Fig. 5. (a) EQE for the optimized 3J-PSC with optimal bandgap and the fabricated cell in Ref. [13] (b) PCEs of Ref. [13], Optimized 3J-PSC and the optimized 3J-PSC with ideal R_{sh} and R_s.

Optics EXPRESS

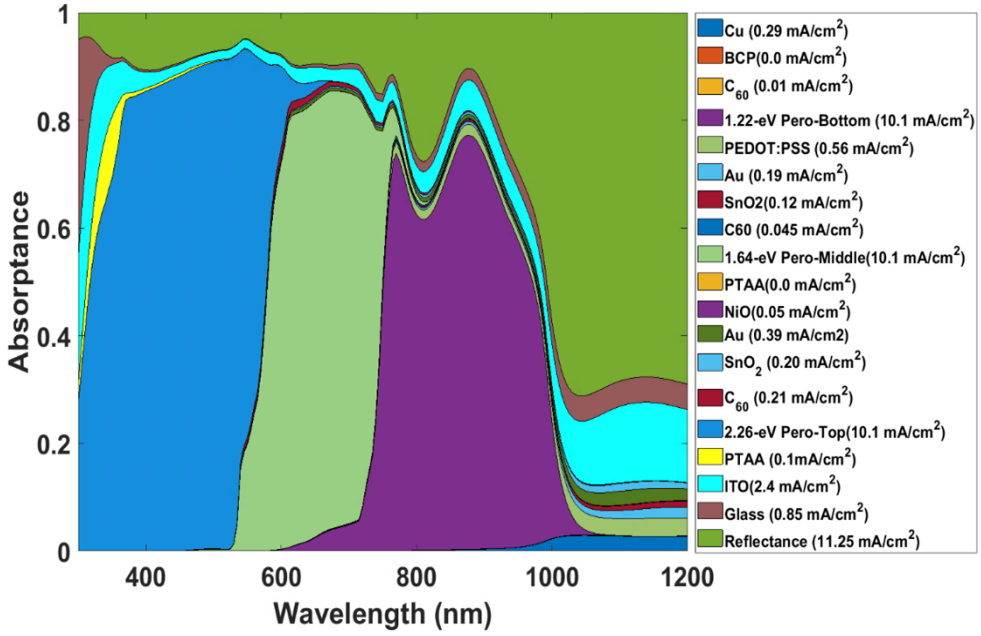

Fig. 6. Absorbance and current analysis (current losses resulting from parasitic absorption and reflection) inside each layer of the optimized 3J-PSC with the perovskite absorbers bandgaps of 2.26 eV, 1.64 eV, and 1.22 eV.

4.3. Electrical optimization (V_{OC}/E_G ratio)

This study aims to optimize the V_{OC}/E_G ratio to increase the PCE of the 3J-PSC under investigation. The open-circuit voltage (V_{OC}) is raised from 3.072 V to 3. 686 V to change the $q \times V_{OC-\ tandem}$ / ($E_{G-\ bottom} + E_{G-middle} + E_{G-top}$) ratio from 0.6 to 0.72. Figure 7 displays the heat map table of optimized 3J-PSC with J_{SC} on the x-axis and V_{OC}/E_G ratio on the y-axis at a constant FF of 81.1%. This figure shows that increasing the J_{sc} and/or the V_{OC}/E_G ratio leads to an increase in the PCE, which can reach a maximum value of 36%. It is worth highlighting that the V_{OC}/E_G ratio is changed based on the values from the literature, where the recent studies reported that a certified 3J-PSC with a V_{OC}/ E_G ratio of 0.65 had a PCE of 23.4% [14] and the cell reported in [13] with a ratio of 0.58 had a PCE of 20.1%. Therefore, the reported cell at the same V_{OC} /E_G ratio of 0.65 as in [14] offers a PCE of 32.6% with a relative enhancement of 39.9%. Similarly, our optimized cell with the same V_{OC} /E_G ratio of 0.6, as in [13], shows a PCE of 29.15 with a 45% improvement. Further increasing the V_{OC}/E_G ratio up to 0.72 will increase the PCE to 36%. This indicates a significant scope for improvement in 3J-PSC. Specifically, exploring novel approaches to enhance electrical parameters through developing new passivation and charge carrier extraction layers, coupled with meticulous minimization of series resistance losses, is expected to elevate the PCE of the next generation of 3J-PSC. Table S5 in Supplement 1 shows the electrical parameters used for the perovskite subcells to produce results in Fig. 7.

Optics EXPRESS

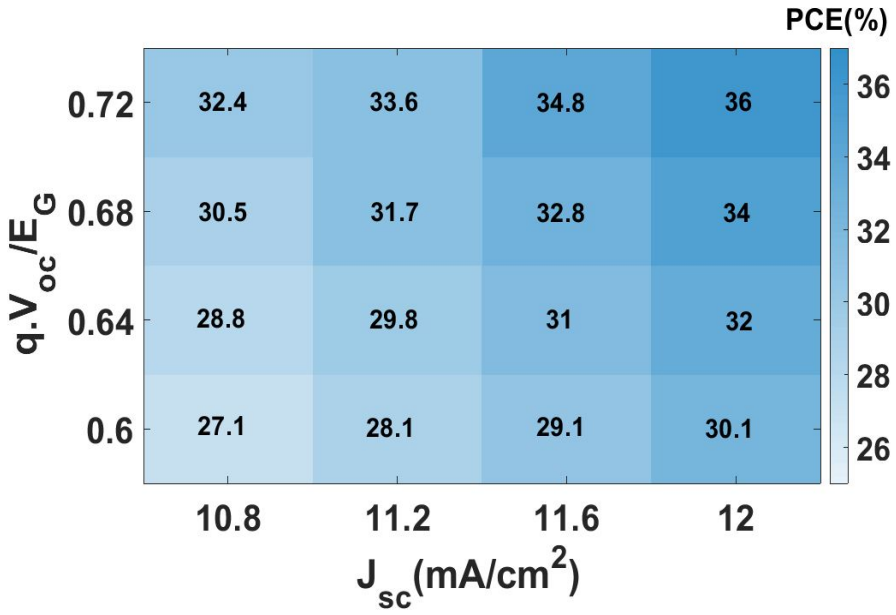

Fig. 7. Heat map table showing the PCE of optimized all 3J-PSC for incremental improvement of J_{SC} on one x-axis and $q{\cdot}V_{\mathrm{OC-tandem}}\,/(E_{G-top}+E_{G-middle}+E_{G-bottom})$ ratio on the y-axis at constant FF of 81.1%

4.4. *Fabrication tolerance and sensitivity analysis for optimized 3J-PSC*

While the techniques for fabricating 2T-3J-PSC are established, nano-scale processes always exhibit potential fabrication tolerances. Therefore, a dedicated study is conducted to quantify the sensitivity of the PCE to slight deviations in critical parameters such as perovskite layer absorber thicknesses. The sensitivity study is performed by variations of ± 10 nm in the optimal dimension of each perovskite absorber, while the other parameter thicknesses are held constant at their optimum values of TCO:IO:H = 180 nm and ARC 88 nm. The summary of the tolerance study is listed in Table 3. It can be seen from this study that the suggested optimal 2T-3J-PSC maintains a stable performance and still maintains high PCE even when each parameter is varied between ±10 nm % of its optimized value, demonstrating its high robustness for fabrication deficiency and reassuring us of its consistent performance.

Table 3. Fabrication Tolerance for the optimized 3J-PSC

Layer	Optimum Thickness (nm)	PCE		
		Optimized	**+1%(+10 nm)**	**-1%(-10 nm)**
Top: Perov.	**996**	**27.07%**	**27.11%**	**27.03%**
Middle: Perov.	**996**	**27.07%**	**27.07%**	**27.07%**
Bottom - Perov.	**1000**	**27.07%**	**27.07%**	**27.07%**

4.5. *Bandgap optimization under realistic outdoor conditions (ROCs)*

The analysis of optimized tandem stacks under STCs is interesting from a research lab perspective, as it can be universally utilized to characterize SCs experimentally. However, for real-world applications, which should be the long-term focus of SC development, the annual energy yield at a specific deployment location (ROCs) is much more significant for financial and engineering

Optics EXPRESS

feasibility analysis. This study aims to identify the optimum bandgap combination for top and middle perovskite absorbers under ROCs in Phoenix. In this context, we analyze the impact of variation in the combination of the middle and top perovskite layers' bandgaps on top of the perovskite bottom subcell with a 1.22 eV bandgap on PCE of 3J-PSC. In this investigation, the top cell bandgap varies from 1.90 eV to 2.3 eV, and the middle layer is changed from 1.48 eV to 1.68 eV. The perovskite bandgaps and thicknesses of all the stack layers in Fig. 1(a) will be changed simultaneously using optimization techniques to maximize the energy yield (EY). Figure 8 shows the variation of the EY with the combination of the middle and top perovskite layers under ROCs in Phoenix. It can be noted from this figure that the top layer bandgap increases from 1.9 eV to 2.18 eV, and the EY also increases. However, when the top layer bandgap is further increased to 2.22 eV, the EY is decreased again. On the other hand, as the middle layer bandgap is increased from 1.48 eV to 1.64 eV, the EY also increases. Nevertheless, the EY decreases if the bandgap is further increased to 1.68 eV. The optimum top and middle perovskite bandgaps are 2.18 eV and 1.64 eV, respectively, with a maximum EY of 538.02 KWh/m^2**.** It is worth noting that the top layer bandgap under ROCs is lower than under STCs due to a bluer, more shifted spectrum in ROCs. Table S6 in the Supplement 1 shows the thicknesses for each bandgap's combination. Therefore, the three perovskite absorbers bandgaps, 2.18 eV, 1.64 eV, and 1.22 eV, respectively, will be used in the following simulation study.

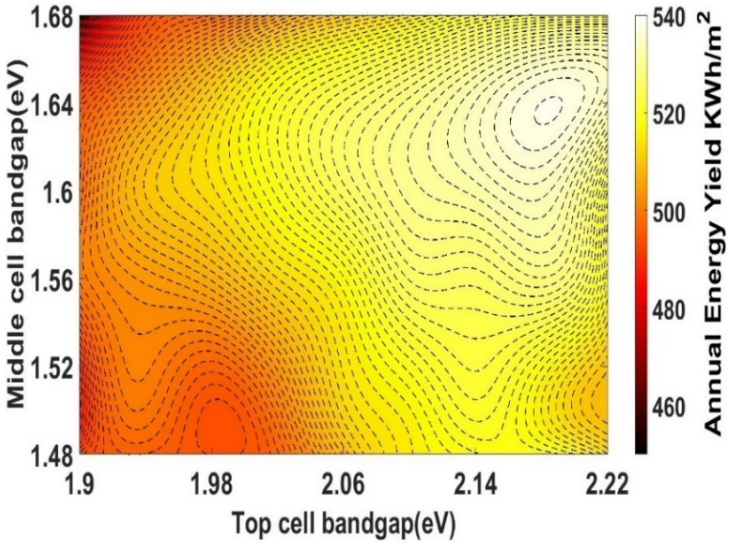

Fig. 8. Annual energy yield of the reported all 3J-PSC as a function of the bandgap combinations of top and middle perovskite layers on the top of perovskite base absorber with a fixed bandgap of 1.22 eV under ROCs in Phoenix

4.5.1. Energy yield evaluation in diverse climatic conditions

Next, we investigate how much the 3J-PSC performance is influenced by changes in the spectral composition of the sunlight, as compared to SJ Si-SC. We will achieve this by calculating the annual EY for different locations in the United States that cover several climatic zones. Figure 9(a) shows the annual EY of SJ Si-SC and the optimized all 3J-PSC in six locations across the United States at V_{OC}/ E_G ratios of 0.6 and 0.72. It can be seen from this figure that increasing the V_{OC}/ E_G ratio from 0.6 to 0.72 leads to an increase in the annual EY, and the optimized cell with optimum bandgaps generates the highest annual EY for all locations, irrespective of the climatic condition. At the same time, the reference Si-SC always shows a lower EY. The highest

Optics EXPRESS

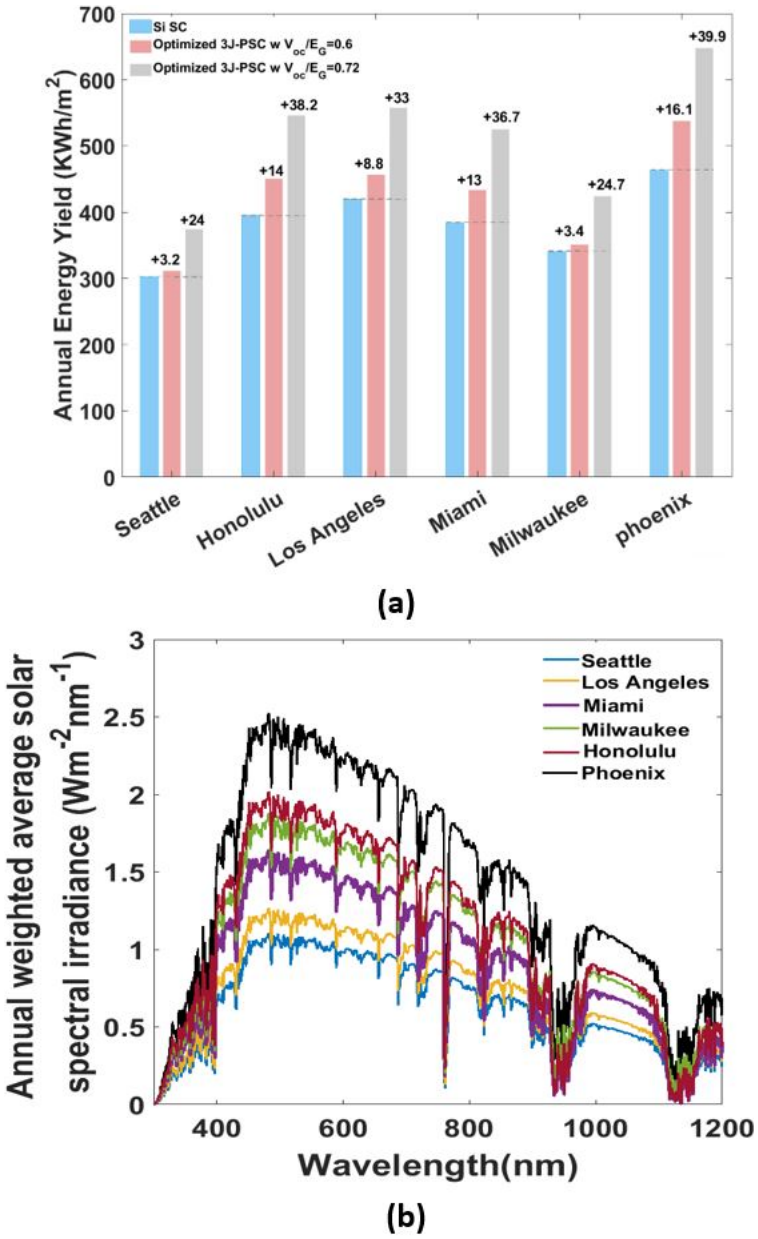

Fig. 9. (a) Simulated annual energy yield (EY) of the c-Si SJ-SC and optimized all 3J-PSC in six different locations in the USA (b) Annual weighted average solar spectral irradiance in six cities represents different climate conditions.

EY of 648.2 KWh/m^2 is obtained at Phoenix at a V_{OC}/ E_G ratio of 0.72, with an improvement of 39.9% compared to the Si SC counterpart. The lowest EY is recorded in Seattle at 374.6 KWh/m^2, with an enhancement of 24% compared to Si SC. It is crucial to highlight that the EY varies significantly based on the climatic zones of the locations. The highest EY for optimized 3J-PSC SC is observed in Phoenix because it shows a drier and sunnier climate with fewer clouds, which allows more direct sunlight to reach solar panels, thus contributing to increased energy

Optics EXPRESS

yield. In contrast, Seattle has a higher frequency of overcast and rainy days, leading to more diffuse sunlight and reduced direct sunlight exposure. This leads to a reduced average current matching. This is consistent with the annual weighted average solar spectral irradiance of the six locations shown in Fig. 9(b), where the lowest annual weighted average solar spectral irradiance is observed in Seattle and the highest in Phoenix and Honolulu. Table S7 in the Supplement 1 displays the layer's thicknesses in each location.

5. Conclusion

This paper investigates the impact of different bandgap combinations on light absorption and power conversion efficiency of the solar cell, and it also explores how changing the test conditions from standard to realistic conditions can affect the overall performance of 3J-PSC, where changing the climate conditions, such as temperature, humidity, and light exposure, will influence the annual energy yield. To achieve this goal, the optimization algorithm, coupled with the in-house energy yield code, is employed to determine the optimum bandgaps and the stack thicknesses of perovskite absorber layers, transparent conductive oxide, hole transport layer, and recombination junctions. The optimized cell offers a PCE of 27.1%, which exceeds what has been reported and certified in the literature. Furthermore, electrical optimization has been carried out to enhance the cell's performance further. The reported cell with a V_{OC}/ E_G ratio of 0.72 shows a PCE of 36%. Last, we examined the optimal bandgaps and thicknesses under realistic outdoor conditions in Phoenix. The cell with optimized bandgaps and thicknesses offers a high annual energy yield of 648.2 KWh/m^2 in Phoenix. The optimized cell is compared with silicon SC in several realistic locations. The proposed 3J-PSC outperformed performance in all locations, with an enhancement in the annual energy yield varying from 39.9% to 24% in Phoenix and Seattle, respectively.

Funding. Helmholtz Association (MTET (38.01.05)), Solar Technology Acceleration Platform (Solar TAP)).

Acknowledgment. The authors thank the Helmholtz Association MTET program (Materials and Technologies for the Energy Transition)—Topic 1—Photovoltaics (38.01.05). The Helmholtz Association has supported part of this work through the Solar Technology Acceleration Platform (Solar TAP).

Disclosures. The authors declare no conflicts of interest.

Data availability. The complete code of the EYcalc modelling platform used for this work and the related datasets have been uploaded to GitHub [23].

Supplemental document. See Supplement 1 for supporting content.

References

1. N. S. Lewis, "Toward cost-effective solar energy use," Science **315**(5813), 798–801 (2007).
2. H. Shen, T. Duong, Y. Wu, *et al.*, "Metal halide perovskite: a game-changer for photovoltaics and solar devices via a tandem design," Sci Technol Adv Mat **19**(1), 53–75 (2018).
3. K. Yoshikawa, H. Kawasaki, W. Yoshida, *et al.*, "Silicon heterojunction solar cell with interdigitated back contacts for a photoconversion efficiency over 26%," Nat. Energy **2**(5), 17032 (2017).
4. A. Polman, M. Knight, E. C. Garnett, *et al.*, "Photovoltaic materials: Present efficiencies and future challenges," Science **352**(6283), aad4424 (2016).
5. F. Meillaud, A. Shah, C. Droz, *et al.*, "Efficiency limits for single-junction and tandem solar cells," Sol. Energy Mater. Sol. Cells **90**(18-19), 2952–2959 (2006).
6. F. Dimroth, M. Grave, P. Beutel, *et al.*, "Wafer bonded four-junction GaInP/GaAs//GaInAsP/GaInAs concentrator solar cells with 44.7% efficiency," Prog. Photovoltaics **22**(3), 277–282 (2014).
7. P. T. Chiu, "35.8% space and 38.8% terrestrial 5J direct bonded cells," in *2014 IEEE 40th Photovoltaic Specialist Conference (PVSC)*, 2014), 0011–0013.
8. S. Yadav, M. A. Kareem, H. K. Kodali, *et al.*, "Optoelectronic modeling of all-perovskite tandem solar cells with design rules to achieve >30% efficiency," Sol. Energy Mater. Sol. Cells **242**, 111780 (2022).
9. A. Kojima, K. Teshima, Y. Shirai, *et al.*, "Organometal Halide Perovskites as Visible-Light Sensitizers for Photovoltaic Cells," J. Am. Chem. Soc. **131**(17), 6050–6051 (2009).
10. R. Lin, K. Xiao, Z. Qin, *et al.*, "Monolithic all-perovskite tandem solar cells with 24.8% efficiency exploiting comproportionation to suppres Sn(ii) oxidation in precursor ink," Nat. Energy **4**(10), 864–873 (2019).
11. G. E. Eperon, M. T. Hörantner, H. J. Snaith, *et al.*, "Metal halide perovskite tandem and multiple-junction photovoltaics," Nat. Rev. Chem. **1**(12), 0095 (2017).

Optics EXPRESS

12. J. Wang, V. Zardetto, K. Datta, *et al.*, "16.8% Monolithic all-perovskite triple-junction solar cells via a universal two-step solution process," Nat. Commun. **11**(1), 5254 (2020).
13. K. Xiao, J. Wen, Q. Han, *et al.*, "Solution-Processed Monolithic All-Perovskite Triple-Junction Solar Cells with Efficiency Exceeding 20%," ACS Energy Lett. **5**(9), 2819–2826 (2020).
14. J. Wang, L. Zeng, D. Zhang, *et al.*, "Halide homogenization for low energy loss in 2-eV-bandgap perovskites and increased efficiency in all-perovskite triple-junction solar cells," Nat. Energy **9**(1), 70–80 (2023).
15. N. Shrivastav, J. Madan, M. Khalid Hossain, *et al.*, "Design and simulation of three-junction all perovskite tandem solar cells: A path to enhanced photovoltaic performance," Mater. Lett. **362**, 136169 (2024).
16. A. D. Vos, "Detailed balance limit of the efficiency of tandem solar cells," J. Phys. D: Appl. Phys. **13**(5), 839–846 (1980).
17. M. Hussein, "Optimal design of vertical silicon nanowires solar cell using hybrid optimization algorithm," J. Photon. Energy **8**(02), 1 (2017).
18. S. Katoch, S. S. Chauhan, V. Kumar, *et al.*, "A review on genetic algorithm: past, present, and future," Multimed Tools Appl **80**(5), 8091–8126 (2021).
19. J. Kennedy and R. C. Eberhart, "Particle swarm optimization," in *Proceedings of ICNN'95 - International Conference on Neural Networks*, (IEEE, Perth, WA, Australia, 1995), pp. 1942–1948.
20. E. Rashedi, H. Nezamabadi-pour, S. Saryazdi, *et al.*, "GSA: A Gravitational Search Algorithm," Inf. Sci. **179**(13), 2232–2248 (2009).
21. S. Mirjalili and S. Z. M. Hashim, "A new hybrid PSOGSA algorithm for function optimization," in *2010 international conference on computer and information application*, (IEEE, 2010), 374–377.
22. R. Schmager, "EYcalc-Energy yield calculator for multi-junction solar modules with realistic irradiance data and textured interfaces," Zenodo, 2021, https://zenodo.org/records/4696257.
23. R. Schmager, M. Lagenhorst, J. Lehr, *et al.*, "EYcalc," Github, 2022, https://github.com/PerovskitePV/EYcalc.
24. S. Mirjalili, "Hybrid Particle Swarm Optimization and Gravitational Search Algorithm (PSOGSA)," MATLAB Central File Exchange, 2024, https://www.mathworks.com/matlabcentral/fileexchange/35939-hybrid-particle-swarm-optimization-and-gravitational-search-algorithm-psogsa.
25. V. Veerasamy, N. I. Abdul Wahab, R. Ramachandran, *et al.*, "Automatic load frequency control of a multi-area dynamic interconnected power system using a hybrid PSO-GSA-tuned PID controller," Sustainability **11**(24), 6908 (2019).